Mon. Not. R. Astron. Soc. **000**, 1–10 () Printed 7 October 2004 (MN LATEX style file v2.2)

# The Galaxy Cluster Abell 3581 as seen by *Chandra*

R.M. Johnstone[1⋆], A.C. Fabian[1], R.G. Morris[1] and G.B. Taylor[2]
[1]*Institute of Astronomy, University of Cambridge, Madingley Road, Cambridge CB3 0HA*
[2]*NRAO, Socorro, NM 87801, USA*



Received

**ABSTRACT**

We present results from an analysis of a *Chandra* observation of the cluster of galaxies Abell 3581. We discover the presence of a point-source in the central dominant galaxy which is coincident with the core of the radio source PKS 1404-267. The emission from the intracluster medium is analysed, both as seen in projection on the sky, and after correcting for projection effects, to determine the spatial distribution of gas temperature, density and metallicity. We find that the cluster, despite hosting a moderately powerful radio source, shows a temperature decline to around 0.4 $T_{\rm max}$ within the central 5 kpc. The cluster is notable for the low entropy within its core. We test and validate the XSPEC `projct` model for determining the intrinsic cluster gas properties.

**Key words:** galaxies: clusters: general – galaxies: clusters: individual: Abell 3581 – intergalactic medium – X-rays: galaxies: clusters

## 1 INTRODUCTION

Abell 3581 is a nearby ($z \sim 0.0218$), richness class 0, cluster of galaxies. The central dominant galaxy IC 4374 has an extensive optical emission-line filament system (Danziger & Focardi 1988, Johnstone, Fabian & Nulsen 1987) like that seen around the central galaxy in more massive clusters (e.g. the Perseus cluster, Conselice et al. 2001).

Abell 3581 was previously studied in X-rays, using data from the *ROSAT* and *ASCA* satellites by Johnstone, Fabian & Taylor (1998) who found that it had a cool intracluster medium (ICM) with $kT \sim 2$ keV, and a short radiative cooling time throughout its core. Those data admitted a classical cooling flow with a significant amount of intrinsic absorption.

Recently, (e.g. Peterson et al. 2001, Johnstone et al. 2002, Peterson et al. 2003, Kaastra et al. 2004, Sanders et al. 2004) it has been shown that clusters which have short central cooling times have much less gas at temperatures below about a third of the ambient cluster temperature compared with that expected from simple cooling. This inconsistency between theory and observations has led to the proposal of many different mechanisms to reheat the cooling gas. One popular subset of these heating models appeals to energy input from the active nucleus in the central dominant galaxy, which is usually found to harbour a radio source (Burns et al. 1997).

The central dominant galaxy in Abell 3581 hosts the powerful radio source PKS 1404-267. Since this is a cool cluster with a powerful radio source at its centre, it might be expected that if active galactic nuclei (AGN) are able to heat the ICM in clusters, this source might show the effects more clearly than richer clusters. However, although we will show that the ICM does not have significant amounts of gas below a temperature of $kT \sim 0.8$ keV, there seems to be no other clear evidence for heating of the ICM by the AGN.

We note that Abell 3581 has a similar mean temperature and luminosity to the cluster Abell 1983 which was recently studied with *XMM-Newton* by Pratt & Arnaud (2003). The properties of the inner core of Abell 3581 are however quite different from those of Abell 1983.

## 2 OBSERVATIONS

We present a *Chandra* observation (Obsid: 1650, Sequence number: 800118) of the cool cluster Abell 3581 which was made on 2001 June 7 with the S3 back-illuminated detector in the ACIS-S instrument.

Data processing has been done using the CIAO package available from the *Chandra* X-ray Centre while spectral fitting used the XSPEC package (Arnaud 1996). The events file was reprocessed to apply the most appropriate gain file to this observation, which was made with a focal plane temperature of -120C, and to remove periods of bad background flaring. This resulted in a total of 7165s of good on-source exposure from the nominal 7260s observation. The PI column of the resulting events file was corrected for the temporal dependence of the gain by using the CORR_TGAIN package made available by Alexey Vikhlinin[1].

Analysis of the cluster emission used data processed for best

⋆ E-mail: rmj@ast.cam.ac.uk

[1] `http://cxc.harvard.edu/cont-soft/software/corr_tgain.1.0.html`

background discrimination from the 'very faint' data mode. Analysis of the point-source used standard 'faint mode' processing since the point-source counts are moderately affected by pileup.

Throughout this paper, we adopt a redshift for Abell 3581 of $z = 0.0218$ (Johnstone, Fabian & Taylor 1998) and a cosmology that assumes a flat universe with $H_0 = 70\,\mathrm{km\,s^{-1}}$ and $\Omega_m$=0.3. We use N Wright's web page[2] to calculate that the angular diameter distance to this source is 90.9 Mpc and its luminosity distance is 94.9 Mpc. The linear scale is 441pc per arcsec. Wherever we quote uncertainties these are at the $1\sigma$ level, unless explicitly stated otherwise. In general we have used the chi-square statistic to assess goodness of fit and tests for significance of additional parmeters, but have used the XSPEC implementation of Cash's C-statistic to determine parameter uncertainties and confidence regions[3].

Recently Barnes & Nulsen (2003) have carried out a detailed investigation of the fluctuations in the Galactic foreground absorption equivalent Hydrogen column density in the direction of this cluster. They reference two absolute measurements from the literature: Stark et al. (1992), using a 2-degree beamsize find $N_{\rm H} = 4.5 \times 10^{20}\,\mathrm{cm^{-2}}$, while Hartmann & Burton (1997) using a 35 arcmin beam found $N_{\rm H} = 4.1 \times 10^{20}\,\mathrm{cm^{-2}}$. In their investigation of *fluctuations* in the value of $N_{\rm H}$ towards this cluster, using new data from the Australia Telescope Compact Array, Barnes & Nulsen (2003) find that at the $5\sigma$ level fluctations larger than $\pm 6.2 \times 10^{19}\,\mathrm{cm^{-2}}$ are ruled out. Throughout this paper we adopt therefore the value of $N_{\rm H} = 4.1 \times 10^{20}\,\mathrm{cm^{-2}}$ (from the more compact beam observation) as the value of the Galactic foreground absorption.

In Fig. 1 we show the *Chandra* X-ray image of the central $\sim$3.5x3.5 arcmin region of Abell 3581 in the 0.3-3.0 keV band. The X-ray events were binned to have 1 arcsec pixels before being adaptively smoothed. A clear detection of an X-ray emitting active nucleus is seen close to the centre of the cluster X-ray emission.

The presence of the radio source PKS 1404-267 at the centre of this cluster has been known since the 1960s, but the *Chandra* image shows, for the first time, that there is an X-ray emitting point source associated with it. In Fig. 2 we show a close-up of the X-ray image (which has been unsharp masked) with a map of the radio source obtained from the National Radio Astronomy Observatory[4] archive overlaid in contours. This 700s 20cm (1477 MHz) radio image was taken on 1987 September 21 with the VLA in the "A" configuration. The peak flux density is 396 mJy/beam with a synthesised beam of $3.34\times1.14$ arcsec in position angle $-27$ degrees. Clear cavities in the X-ray emission are seen to the East and West of the nucleus, coincident with the lobes of the radio source.

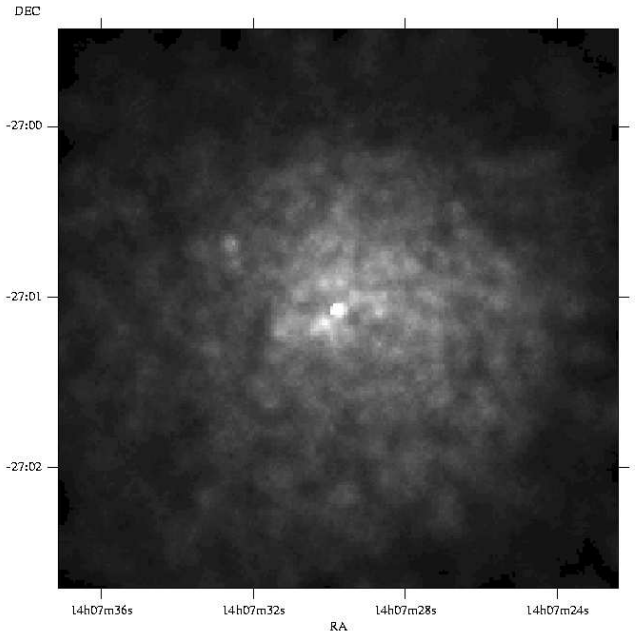


**Figure 1.** *Chandra* X-ray image of Abell 3581 in the 0.3-3 keV band. The data have been binned to 1 arcsec pixels and adaptively smoothed.

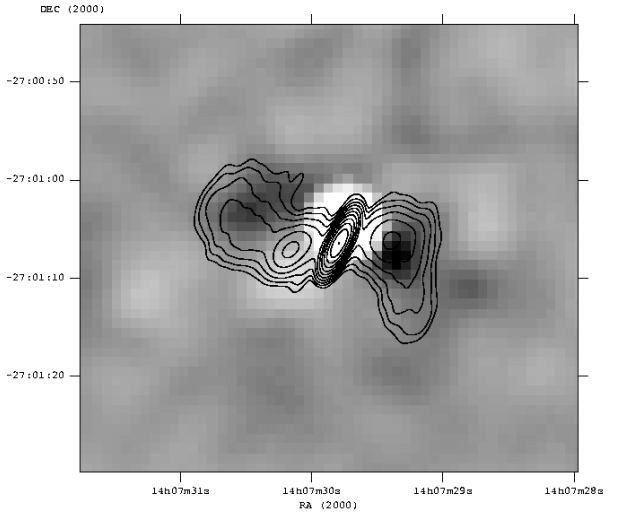


**Figure 2.** Unsharp masked X-ray image of Abell 3581 (greyscale) with the 20cm VLA map of the PKS 1404-267 radio source overlaid. There are 12 contours in the radio map spaced equally in logarithmic steps between 0.7 mJy/beam and 390 mJy/beam.

## 3 THE X-RAY POINT SOURCE

The X-ray point source is located approximately at RA(2000)=14:07:29.8, Dec(2000)=$-$27:01:04. We extracted a spectrum from a circular region of radius 1.8 arcsec centred on the point source. The major component of the background for this source is the surrounding cluster emission, so in this case, we extracted the background spectrum from an annular region surrounding the nucleus with radius between 1.97 and 3.94 arcsec. Spectra were rebinned to have a minimum of 20 counts per bin.

Redistribution matrices and ancilliary response functions were computed using calibration files from the *Chandra* calibration database version 2.26. This release corrects a previous one-channel offset error in the FITS embedded function file and incorporates a correction for the degradation in low-energy quantum efficiency due to the build-up of a contaminant on the filter wheel.

We have modelled the spectrum of the point source as a power-law modified, initially, only by Galactic absorption. Preliminary fit results were input to the WebPIMMS[5] count rate simulator which

[2] `http://www.astro.ucla.edu/~wright/CosmoCalc.html`
[3] `http://xspec.gsfc.nasa.gov/docs/xanadu/xspec/manual/manual.html`
[4] The National Radio Astronomy Observatory is operated by Associated Universities, Inc., under cooperative agreement with the National Science Foundation.
[5] `http://heasarc.gsfc.nasa.gov/Tools/w3pimms.html`

suggested that pileup was important at approximately the 8 per cent level. This is at a level where pileup is starting to become significant, so all subsequent fitting of the point source was done including the XSPEC implementation of the pileup model of Davis (2001).

The best fit using the pileup model applied to a power-law with the Galactic absorption column density fixed at $4.1 \times 10^{20}$ cm$^{-2}$ gives a chi-square value of 11.2 for 20 degrees of freedom. Allowing the absorption to be freely fitted does not significantly decrease the chi-square value.

In order to estimate the power-law index and its statistical uncertainties we use Cash's C-statistic (Cash 1979, implemented in the XSPEC `cstat` command) since there are many PI bins with the minimum number (20) of counts. The best fitting power-law model has a photon number index of $2.28^{+0.11}_{-0.15}$, a 2-10 keV flux of $2.16 \times 10^{-13}$ erg cm$^{-2}$ s$^{-1}$ and a 2-10 keV (rest frame) luminosity corrected for Galactic absorption of $2.35 \times 10^{41}$ erg s$^{-1}$. The 0.1-10 keV luminosity is $1.08 \times 10^{42}$ erg s$^{-1}$.

We can calculate the expected luminosity of the point source, assuming that it is a black hole accreting according to standard Bondi theory (Bondi 1952) with a radiative efficiency of 10 per cent. The bolometric luminosity is given by:

$$L_{\rm acc} = \frac{8.50 \times 10^{26} M_{\rm bh} n_{\rm e}}{T^{1.5}} \,{\rm erg\,s^{-1}},$$

where $M_{\rm bh}$ is the mass of the black hole in solar masses, $n_{\rm e}$ is the electron density in cm$^{-3}$, and $T$ is the accreting gas temperature in keV.

The work of Bettoni et al. (2003) gives the mass of the black hole in PKS 1404-267 as being in the range $8.5 - 9.5 \times 10^8$ M$_\odot$ while the temperature and density of our innermost spatial bin calculated from the `projct` model in section 4.2 are $kT = 0.81$ keV and $n_{\rm e} = 0.066\,{\rm cm^{-3}}$ respectively. These values yield a bolometric luminosity of $6.9 \times 10^{43}$ erg s$^{-1}$. If we assume that most of the accretion luminosity comes out in the 0.1-10 keV band then the ratio of observed to expected luminosity is 0.016. The nucleus is underluminous by a factor of $\sim 64$. This is much larger than any expected bolometric correction ($< \times 10$). We note also that part of the 'point' source may actually be the innermost parts of the radio jets, at the nucleus itself.

We note that appropriate values of temperature and density to put into the formula for the luminosity are those pertaining at the accretion radius:

$$R_{\rm acc} \sim \frac{GM_{\rm bh}}{c_{\rm s}^2},$$

where $c_{\rm s}$ is the sound speed, or

$$R_{\rm acc} = \frac{3.705 \times 10^{-11} M_{\rm bh}}{T}.$$

For the innermost measured value of $T$ in our data $R_{acc} = 0.04$ kpc, which is much closer to the nucleus than our innermost bin can resolve (5 kpc). The work of Di Matteo et al. (2003) on M87 has shown that going in from 5 kpc to the central 1 kpc region the intracluster medium temperature drops by about a factor of two while the density rises by about a factor of three. If similar trends occur in PKS 1404-267 they would increase the expected accretion luminosity, and the discrepancy in the observed value, by more than a factor of 8.

We note that underluminous accretion is also seen in M87 (in the Virgo cluster) by Di Matteo et al. (2003), NGC 6166 (in Abell 2199) by Di Matteo et al. (2001), and the Sombrero galaxy by Pellegrini et al. (2003). However, in these objects the luminosity deficit is rather larger (a factor of $\sim 10^4$) despite the black hole mass being very similar to the one considered here. Possible solutions to the discrepancy are discussed by Di Matteo et al. (2003).

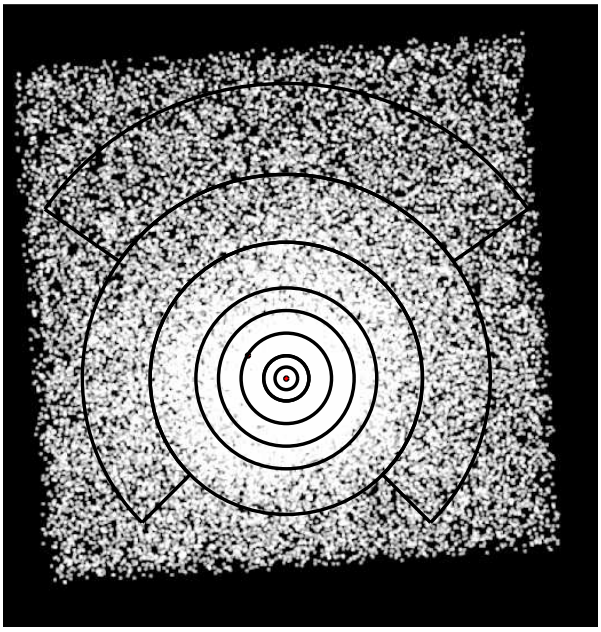

**Figure 3.** Map of the entire S3 chip showing the concentric regions from which spectra were extracted. North is to the top, East to the left.

## 4 CLUSTER EMISSION

Since the surface brightness distribution of the cluster emission is quite circularly symmetric we have extracted spectra from a series of concentric circular annuli centred on the nuclear point source, but excluding counts from that point source, and one other at: RA(2000)=14:07:32.6, Dec(2000)=−27:00:41. Fig. 3 shows the regions used overlaid on an image of the cluster. The radio source is contained almost entirely within the central 5 kpc radius region.

It is not possible to use on-chip data from the same observation as background since the cluster occupies the whole of the S3 chip. We therefore reprocessed the standard background field which most nearly matched the observation date and instrumental configuration to have the same gain file as the target observation. It was not possible to apply the time-dependent gain correction to the background events since the time of observation has been removed from the standard background fields.

Background spectra were extracted from identical chip regions of the reprocessed background file by reprojecting the detector coordinates on to the sky coordinates of the target observation.

Redistribution matrices and ancilliary response files for these spatially extended regions were made using the CIAO 3.0.2 tools MKRMF and MKWARF. Background spectra were extracted from the same regions of the standard background fields as were used to extract the source spectra.

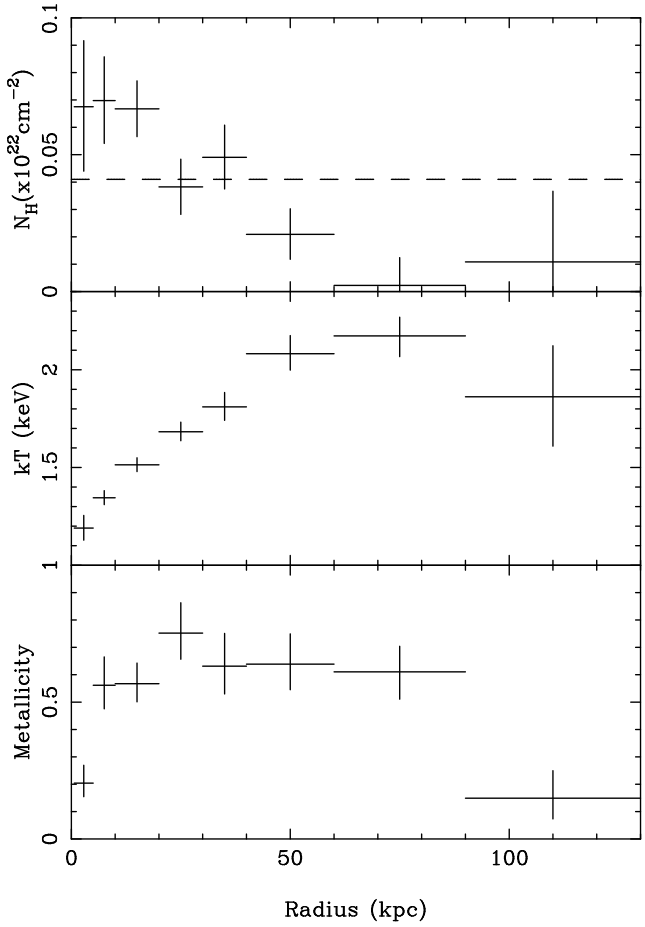


**Figure 4.** Absorption, temperature and metallicity profiles as seen in projection on the sky. The dashed line shows the Galactic column density.

### 4.1 Projected quantities

Single temperature `mekal` (Liedahl et al. 1995) plasma emission models, incorporating freely fitting Galactic absorption were fitted (separately) to the spectra extracted from each annulus. The absorption, temperature, metallicity and normalizations are free parameters for each annulus. In Fig. 4 we show the absorption, temperature and metallicity profiles of the cluster gas derived from these fits.

The absorption measured in the annuli beyond 40 kpc from the nucleus does seem to be slightly systematically low compared with the Galactic column density inferred from 21cm observations which is shown as a dashed line in Fig. 4. This may indicate the level of uncertainty in the model for the correction of the contaminant that has caused the degradation of the low-energy response in the *Chandra* data. We also note that the absorption column density increases roughly linearly from 75 kpc in towards the centre of the cluster by $\sim 7\times10^{20}$ cm$^{-2}$.

Johnstone, Fabian & Taylor (1998) found that the central 3 arcmin region from the ASCA data required a column density of $9^{+2}_{-1}\times10^{20}$ cm$^{-2}$. Such a large value would be consistent with inner 40 kpc or 90 arcsec of the *Chandra* data. However, if the instrumental absorption has been overcorrected in the current analysis then a greater degree of agreement between the ASCA and *Chandra* data is to be expected. The work of Barnes & Nulsen (2003) has shown that the Galactic foreground 21cm emission is constant to within $0.6\times10^{20}$ cm$^{-2}$ ($5\sigma$ upper limit on the fluctuation) in this region of the sky so it is unlikely that variations in Galactic absorption can offer a viable explanation for the increased absorption. The excess absorption seems to be centred on the cluster which would argue for a cluster origin rather than a Galactic origin. The nucleus does not however appear to require any excess absorption (see section 3).

Looking now at the temperature profile, it is clear that the central region of the cluster is cool, at $kT\sim1.2$ keV and that the temperature rises by nearly a factor of $\sim2$ to reach a maximum at 75 kpc from the nucleus. In the one region exterior to this the cluster temperature drops again to near 1.9 keV, although not with high significance. We note that due to the fact that the cluster is not centred on the S3 chip the outermost region is only a partial annulus.

The metallicity in the innermost region has a low value of $\sim0.2$ times the solar value (assuming the solar values of Anders & Grevesse 1989). In the region between 5 and 90 kpc from the nucleus we find a much higher value of $\sim0.6-0.7$ times the solar value. Further out the metallicity falls quickly to $<0.2$ times the solar value again.

In order to assess whether the fall in temperature beyond 90 kpc is cluster wide, we have used an accumulative smoothing / contour binning technique due to J. Sanders (to be described by Sanders et al. 2004, in preparation) to define spatial bins of given signal-to-noise ratio for spectral fitting. This allowed us to drop the assumption of circular symmetry. Briefly, a surface brightness map was produced from the raw counts using a smoothing algorithm which accumulated counts around each pixel until a signal-to-noise ratio of 15 was reached ("accumulative smoothing"). The binning method ("contour binning") then grew bins along directions where the surface brightness is closest to the existing value, until the signal-to-noise ratio exceeded 30. Finally, bins were constrained to have an edge length less than or equal to three times the circumference of a circle of the same area as the bin. Signal-to-noise ratios are calculated taking into account noise in the background spectrum which is extracted from identical regions in chip coordinates from the standard background files.

Spectra were extracted from these regions and binned to 20 counts per spectral bin. New response matrices and ancilliary response functions were made corresponding to these regions which were then fit independently using Cash's C-statistic. The resulting temperature map is shown in Fig. 5.

It is clear now that the south western part of the cluster is systematically hotter than the northern part. Since the outermost annulus comes only from the northern part of the cluster it is not surprising that the outermost annulus has a temperature below the one immediately interior to it since that partial annulus covers the hotter region.

In Fig. 6 we show a close-up of the temperature map of the central region of the cluster with the radio intensity contours overplotted. There is some suggestion that the radio source avoids the the coolest gas, which may be a direct indication that the radio source heats the gas. The precise locations of the boundaries of the individual regions selected for fitting are however somewhat sensitive to the smoothing and signal-to-noise parameters of the contour accretion technique, and are required to follow the surface brightness of the cluster emission.

### 4.2 Correcting for projection effects

We have fit the annular spectra accounting for projection of counts from the exterior regions into interior annuli using the `projct` model in XSPEC, and assuming spherical symmetry. The volumes of the shells sampled by each annulus are calculated from FITS

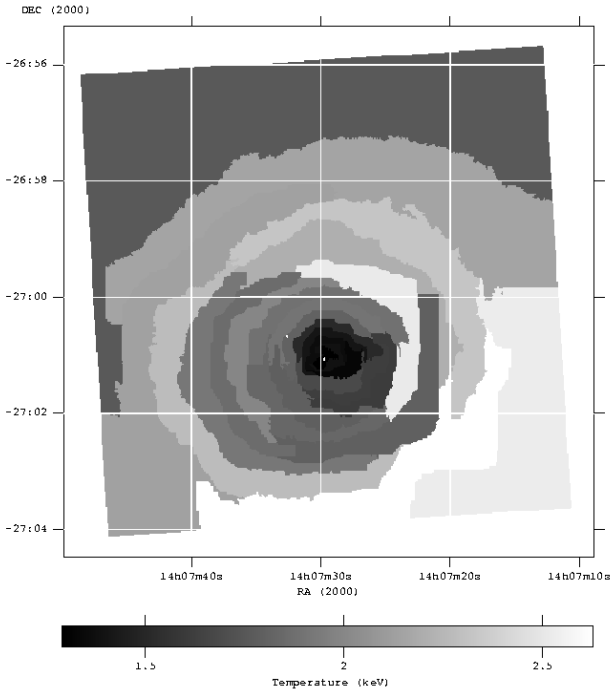


**Figure 5.** X-ray temperature map of Abell 3581.

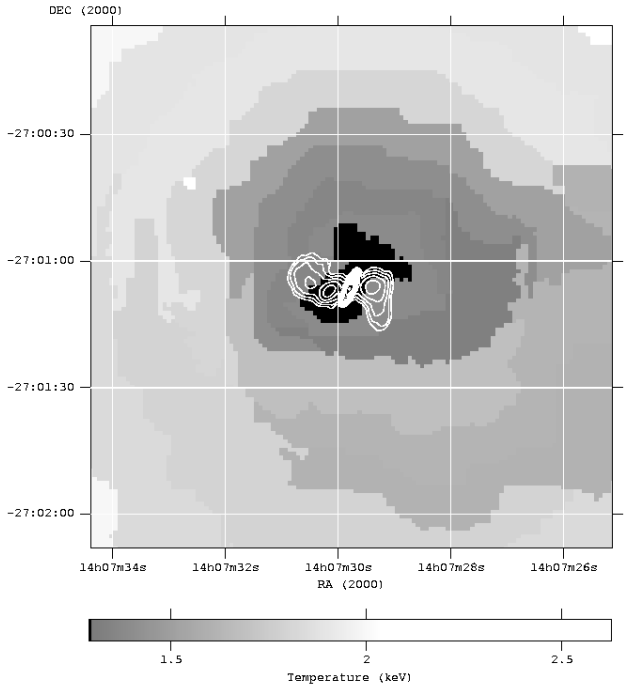


**Figure 6.** X-ray temperature map of the central region of Abell 3581 with radio intensity contours overlaid.

header items which describe the inner and outer boundaries of the annuli. We note that the cluster emission extends beyond the outermost annulus of our analysis so that the emitting volume associated with the outermost annulus is too small. This causes too much projection on to the next annulus in, so that the fit to that annulus underestimates its brightness. The resulting effect is minimal beyond

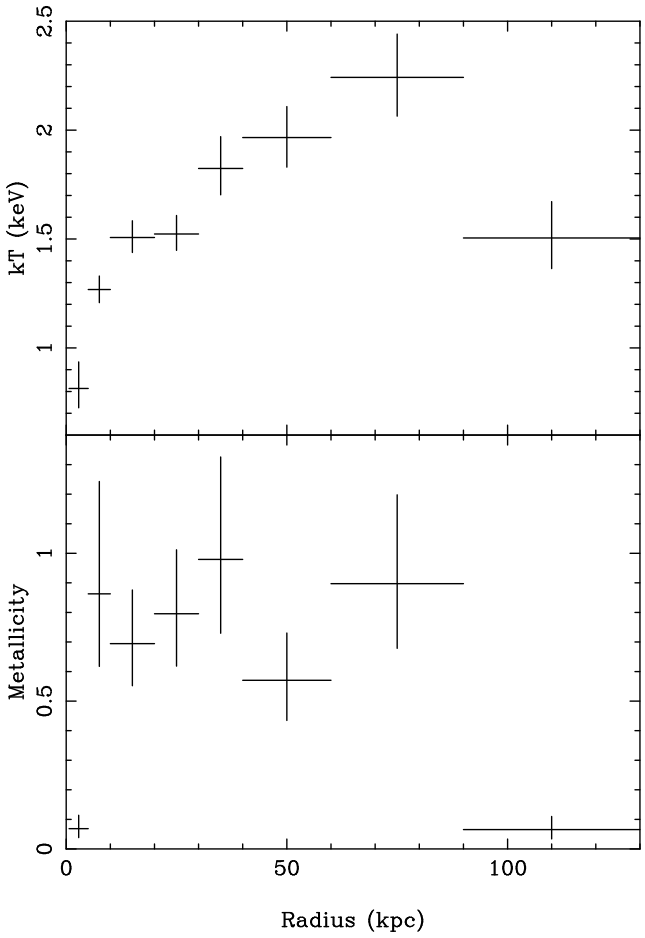


**Figure 7.** Temperature and metallicity profiles for Abell 3581 derived using the `projct` model.

the outer two annuli because the amount of projection is relatively small due to the steep surface brightness profile; see section 4.3.

The model which we have fitted consists of a single temperature `mekal` plasma emission model in which the temperature and metallicity at each radius are freely fit. A single value of the foreground absorption column density is also allowed to fit freely and obtains a value of $3.8 \pm 0.7 \times 10^{20}\,\mathrm{cm}^{-2}$, consistent with that expected from the HI 21cm measurements.

In Fig. 7 we show the temperature and metallicity profiles of the cluster gas derived from these fits accounting for projection. The temperature climbs steadily from 0.8 keV within the central 5 kpc to around 2.25 keV between 60-90 kpc. We note that the intrinsic temperature of the central bin is substantially cooler when taking into account the hotter gas seen in projection against it. In the outermost annulus the temperature drops back to 1.5 keV. Since this region is only a part of an annulus, to the north of the cluster (Fig 3), it is not clear whether this decline in temperature is due to substructure or in fact a coherent property of the cluster.

The metallicity is consistent with 0.8 solar thoughout most of the cluster observed in our dataset. The very innermost region (within 5 kpc, but excluding the nuclear point source) and the region beyond 90 kpc both have much lower values of metal abundance, at around 0.1 times the solar value.

The drop in metallicity in the central bin could be due either to an extended power-law component, or to the iron-bias effect (Buote & Fabian 1999). The iron-bias effect results from fitting a

**Table 1.** Parameters, for the central spatial bin, of models fitted taking into account projection effects. Model 1 is `projct * phabs (mekal)`. Model 2 is `projct * phabs (mekal + po)`. Model 3 is `projct * phabs (mekal + mekal)`. In models 2 and 3 the power-law and second `mekal` components are only present in the innermost spatial bin. Temperatures are given in keV, abundances are relative to the solar value and column densities are in units of $10^{20}$ cm$^{-2}$. "D of F" is the number of degrees of freedom in the fit.

| Model | 1 | 2 | 3 |
|---|---|---|---|
| $kT_1$ | $0.81^{+0.13}_{-0.08}$ | $0.64^{+0.07}_{-0.07}$ | $0.61^{+0.06}_{-0.07}$ |
| $kT_2$ | – | – | $2.50^{+1.11}_{-0.73}$ |
| Abund | $0.07^{+0.07}_{-0.03}$ | $> 0.14$ | $> 0.48$ |
| $N_{\rm H}$ | $4.0^{+0.5}_{-0.5}$ | $3.8^{+0.5}_{-0.5}$ | $3.8^{+0.5}_{-0.5}$ |
| $\chi^2$ | 844.4 | 837.8 | 832.7 |
| D of F | 714 | 712 | 712 |

plasma containing more than one distinct temperature component with a single temperature model.

We have tested for the possibility of there being a spatially extended power-law or a second `mekal` component by adding them (separately) to the baseline `projct * phabs (mekal)` model (Model 1), but only in the central bin. The results of these fits are compared with the baseline model in Table 1. For the test with the power-law component (Model 2), both index and normalization were left as free parameters while for the test with a second `mekal` component (Model 2) we allowed a freely fitting temperature and normalization but tied the metallicity to that of the first `mekal` component. For both tests we found that the metallicity was very poorly constrained and preferred to fit to unphysically large values; we have therefore imposed an upper limit of twice the solar value on this parameter. Indeed the best fit value of the metallicity hits this limit, but we note that allowing much higher values of metallicity does not reduce the value of the chi-square statistic significantly. Our lower limits on the metallicity presented in 1 correspond to an increase of 1.0 in the C-statistic from the value fitted with the metallicity at twice the solar value.

For the model including the power-law component an F-test suggests that there is a 6 per cent chance of obtaining such a significant drop in chi-square if the power-law component is *not* present. For the model including the second `mekal` component an F-test indicates that there is only a 0.7 per cent chance of obtaining such a significant drop in chi-square if the second `mekal` component is *not* present.

We conclude that a two-component `mekal` model is a significantly better fit in the central bin than one with only a single `mekal` component and is preferred over one with an extended power-law component. However, in both of the two-component models the metallicity is sufficiently unconstrained that it becomes consistent with that seen in the second to seventh bins, counting outwards from the centre.

We note that these data are also able to constrain the mass profile of Abell 3581. The results from this work will be presented as part of a larger sample of cluster mass profiles by Voigt & Fabian (2005), in preparation.

### 4.3 Testing the projection correction

We have run a series of tests to check that the `projct` XSPEC model reproduces what is expected when given known synthetic data. We find that it generally gives good results. In Fig. 8, the results of one test which is based upon our dataset are shown.

We start by using the temperature, density and metallicity profiles appropriate for Abell 3581, accounting for projection effects, as determined by the `projct` model. Since the outermost spatial region shows a significant temperature drop we have only used data from the central seven spatial regions in this test. In order to construct a smooth synthetic cluster the density profile was fitted with the sum of two beta profiles, while the temperature profile was fitted with the functional form of Allen et al. (2001). In both cases the outermost point (of the seven) was omitted from the fit (see discussion at the end of this section).

We then constructed a spherically symmetric cluster assuming the ideal gas equation of state. There were 10,000 radial bins equally spaced out to a radius of 2500 kpc, at which point the cluster was truncated.

Spectra appropriate for the physical conditions at each radius were then calculated using the `mekal` plasma code. The emission was integrated along the line of sight to give a projected spectrum at each radius in the cluster. Next the spectra were accumulated radially, in the same annular rings as used in section 4.2, and scaled to the luminosity distance appropriate to Abell 3581 using our adopted cosmology. These spectra were then input to XSPEC, multiplied with a uniform Galactic absorption component, and used to generate synthetic pulse invariant (PI) spectra assuming the same responses and integration time as the Abell 3581 observation. The counts were perturbed following poisson statistics.

The synthetic spectra were then fitted with the `projct` model in XSPEC using the same techniques as in Section 4.2. In Fig. 8 we have overplotted the synthetic cluster profiles for temperature, density and metallicity (dotted lines) with those derived from fitting the PI spectra with the `mekal` and `projct` models, allowing for Galactic absorption (points with error bars). It is clear that the fitted temperature and density points generally match very well with the 'real' synthetic profiles. There appear to be no systematic residuals in the temperature or metallicity profiles. In the density profile we note that the outermost point derived from the `projct` fits is very significantly above the cluster profile. This is because there are counts projected on to this region that cannot be taken into account correctly. The `projct` model requires the projected outer radius for each annulus to be associated with that data set in order to calculate the volume and therefore the projection factors. For the outermost region the volume associated with the counts is wrong in the sense that it is too low. This leads to an overestimate of the surface brightness and density in the outermost annulus. Although this causes too much emission to be subtracted off the next inner annulus, it can be seen that the effect is very small and the errors due to this effect quickly damp out. We therefore have confidence in the projection-corrected results presented in section 4.2, apart from the density in the outermost annulus.

### 4.4 The issue of entropy

In Fig. 9 we show the temperature, electron density and entropy profiles deduced from the fits accounting for projection plotted against the scaled radius. Many authors choose to scale the radial coordinate by $R_{200}$ the radius within which the mean cluster density is 200 times the mean density of the universe. $R_{200}$ has been shown by Cole & Lacey (1996) to be proportional to the virial radius, which is the appropriate scaling quantity in hierarchical self-similar models of structure formation. We have used equation 9 of Sanderson et al. (2003) as an approximation to the virial radius

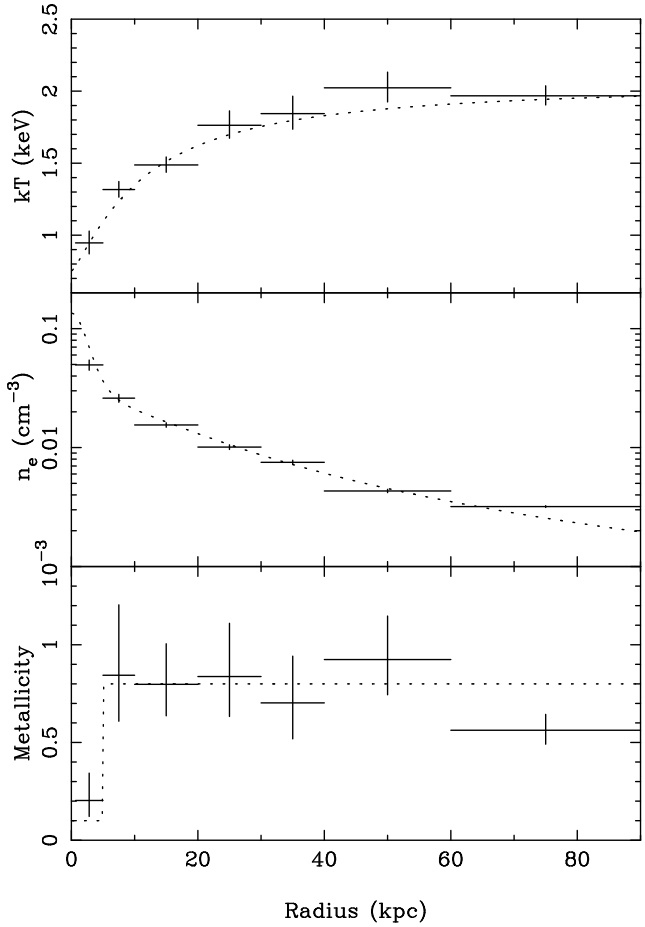


**Figure 8.** Simulated cluster (dotted lines) and parameters derived using the XSPEC `projct` model (crosses).

for our scaling. Using $T_{\rm cluster}$=2 keV (a value which is between that measured in the two outer bins of our data, and within the range measured by Johnstone, Fabian & Taylor 1998, Table 1) we find that the virial radius is 1.11Mpc. Sanderson et al. (2003) have shown that this equation can significantly overestimate $R_{200}$ particularly in small systems with large temperature gradients. Since we have used the maximum temperature in the cluster (at least within the region covered by our data) rather than an emission-weighted average our $R_{200}$ ought to be reasonably accurate.

In calculating the entropy we have used the definition given by Lloyd-Davies et al. (2000), in which the entropy is

$$S = T n_{\rm e}^{-2/3}.$$

The outermost spatial bin at $0.1R_{\rm v}$ is subject to two problems. Firstly, as described in section 4.3 the `projct` model overestimates the density. This translates into too small a value of entropy in that bin. In order to avoid this problem we have estimated the electron density by fitting the other points in the density profile with a double-beta model and extrapolated this to the position of the final spatial bin. This yields an electron density that is a factor of 1.66 times lower than calculated by `projct` for that bin. In Fig. 9 the higher electron density is that determined directly from the `projct` model while the lower value is our corrected value. The entropy point ($S = 120 \pm 13$ keV cm$^2$ ) that we plot at $0.1R_{\rm v}$ is derived from this corrected density.

Secondly, the drop in temperature seen in this bin may not be representative of the cluster averaged profile since it is only a partial annulus and there may be azimuthally dependent temperature structure within the cluster. If the azimuthally averaged temperature profile were to remain flat at the average of the values in the sixth and seventh annuli, counting outwards from the cluster centre, it would have a value of 2.1 keV (however, we note that forcing this value into the `projct` model would reduce the temperature of those inner bins). Values of $kT = 1.8 - 2.2$ keV were found by Johnstone, Fabian & Taylor (1998) from fitting various models to the *ASCA* data from the central 3 arcmin radius region ($0.07R_{\rm v}$) in this source. Using the value of 2.1 keV for the temperature would increase the entropy at $0.1R_{\rm v}$ to 167 keV cm$^2$ . We consider this to be an absolute maximum value for this quantity. We also note that the virial radius increases as the square root of the cluster temperature so it is not strongly affected by changes in the adopted cluster temperature.

The entropy profile for Abell 3581 (as a function of radius scaled by the virial radius) lies well below the profile for clusters with similar temperatures as published by Lloyd-Davies et al. (2000) (taking into account the $S \propto h^{-1/3}$ scaling for the different assumed values of $H_0$). This result stands, despite the presence of the relatively strong Parkes radio source in Abell 3581. The entropy profile for Abell 1983 (Pratt & Arnaud 2003), which has a similar temperature ($kT = 2.1$ keV), has entropy values which are $\sim 40$ keV cm$^2$ higher in the region covered by the *Chandra* data on Abell 3581 (the entropy scaling factor $(1+z)^{-2}T$ expected from self-similar formation models, e.g. Pratt & Arnaud 2003, is the same within 1 per cent for these two objects). Many authors (see e.g. references in Binney & Tabor 1995, Fabian et al. 2001, Churazov et al. 2001) have recently argued that the mechanical heating from an active galactic nucleus with jets can balance the cooling from high density gas in the cluster and thereby prevent the formation of a classical cooling flow. Such heating might be expected to increase the entropy of the clusters, particularly where the gas temperature is cool and the radio source is strong, but this is clearly not the case in Abell 3581.

Ponman et al. (2003) discuss the entropy of intergalactic gas in elliptical galaxies, groups and clusters. Their fig. 4 shows the gas entropy at $0.1R_{200}$ as a function of temperature for 66 virialized systems. Below about 4 keV there is a wide spread in this fiducial entropy. The value of entropy at $0.1R_{\rm v}$ in Abell 3581 calculated from the data at that position in the cluster (with the corrected value for the electron density) is $120 \pm 13$ keV cm$^2$ , or $167 \pm 18$ keV cm$^2$ , if we assume the high value of the temperature in the outermost annulus. By either of these measures, Abell 3581 has an entropy at $0.1R_{\rm v}$ significantly below that for the mean of clusters at 2 keV $\sim 233 \pm 30$ keV cm$^2$ , as shown in fig. 5 of Ponman et al. (2003). Fig. 4 in that same work shows there is a large range in entropy for clusters at 2 keV. Our measured value for Abell 3581 would make it equal to their lowest entropy cluster (Abell 262) at 2 keV. Abell 3581 emphasizes the overall spread in properties of low temperature clusters.

A power-law fit to the entropy as a function of radius ($S = kr^{\alpha}$) gives a slope $\alpha = 0.87 \pm 0.03$. Further including a constant offset in the entropy at zero radius does not produce a significant reduction in the chi-square statistic as determined using an F-test. We note that this is a much flatter slope than expected for pure shock heating of the intracluster gas which is expected to give a slope of $\alpha = 1.1$ (Tozzi & Norman 2001). However, Ponman et al. (2003) have shown, in their fig. 3, that such slopes are usually only seen beyond $0.2R_{\rm v}$, which is outside the region covered by our data.

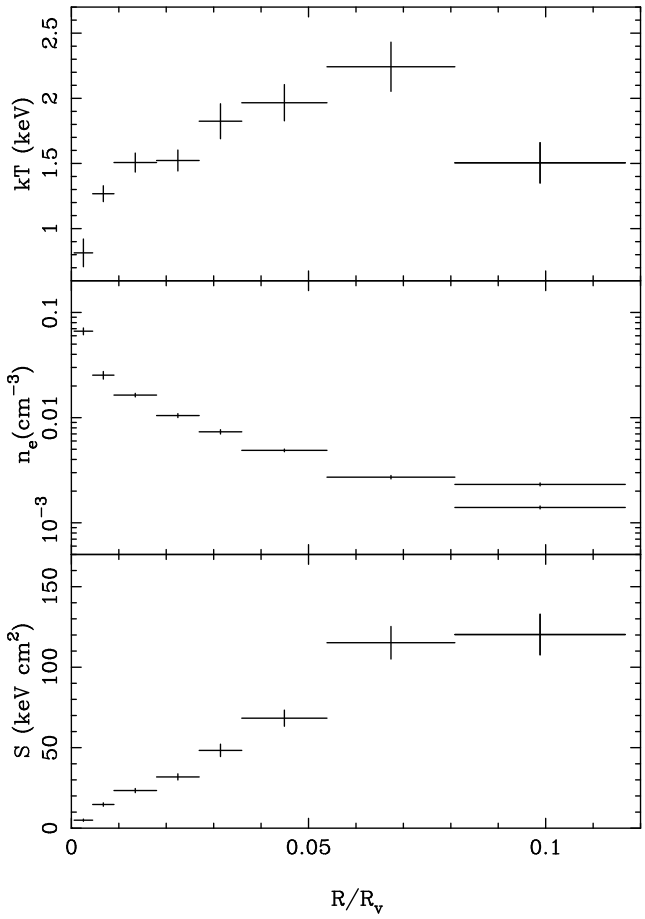


**Figure 9.** Temperature, electron density, and entropy profiles determined from the `projct` model. The radial coordinate has been scaled by the virial radius, 1.11Mpc. There are two points plotted in the electron density profile at $0.1R_v$. The upper point is determined directly from the `projct` value while the lower point is determined from an extrapolation of a double-beta profile fit to the seven inner points. The entropy point plotted at $0.1R_v$ is calculated using the extrapolated fit value for the density. See text for details.

**Table 2.** Parameters of fits to cooling flow region. Model 1 is `phabs (mekal)`. Model 2 is `phabs (mekal + mekal)`. Model 3 is `phabs (mekal + mkcflow)` with the lower temperature fixed at 0.08 keV. Model 4 is `phabs (mekal + mkcflow)` with the lower temperature allowed to fit freely. Temperatures are given in keV, abundances are relative to the solar value, the mass deposition rate $\dot{M}$ is given in solar masses per year and column densities are in units of $10^{20}$ cm$^{-2}$. "D of F" is the number of degrees of freedom in the fit.

| Model | 1 | 2 | 3 | 4 |
|---|---|---|---|---|
| $kT_{\rm upper}$ | $1.68^{+0.02}_{-0.02}$ | $1.86^{+0.05}_{-0.05}$ | $1.83^{+0.04}_{-0.04}$ | $1.90^{+0.06}_{-0.05}$ |
| $kT_{\rm lower}$ | – | $0.86^{+0.09}_{-0.07}$ | 0.08 | $0.60^{+0.11}_{-0.11}$ |
| Abund | $0.53^{+0.03}_{-0.03}$ | $0.75^{+0.06}_{-0.06}$ | $0.74^{+0.07}_{-0.06}$ | $0.76^{+0.07}_{-0.06}$ |
| $\dot{M}$ | – | – | $8.1^{+1.3}_{-1.3}$ | $12.7^{+3.9}_{-2.8}$ |
| $N_{\rm H}$ | $4.4^{+0.4}_{-0.4}$ | $3.9^{+0.5}_{-0.5}$ | $5.1^{+0.5}_{-0.5}$ | $4.0^{+0.5}_{-0.5}$ |
| $\chi^2$ | 338.2 | 303.9 | 306.2 | 302.8 |
| D of F | 205 | 203 | 204 | 203 |

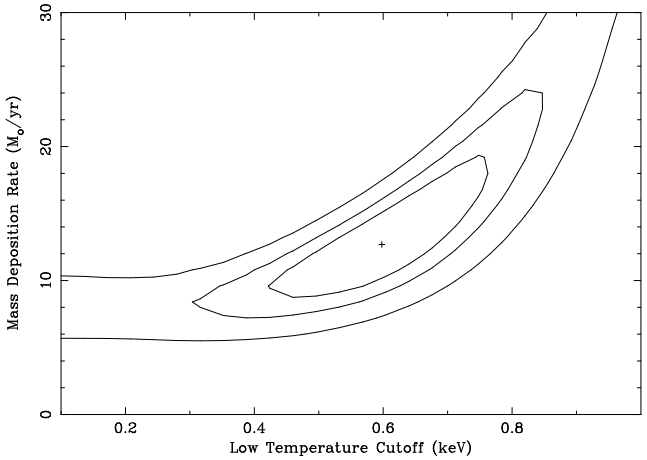


**Figure 10.** Allowed values of mass deposition rate as a function of low temperature cutoff in the cooling gas. Contours are plotted at Δ C-statistic = 2.3, 4.61 and 9.21 which correspond to 68, 90 and 99 per cent confidence regions for two interesting parameters.

The flattening of this slope in the inner regions of clusters may be due to the cooling out of the lower entropy gas.

### 4.5 A classical cooling flow?

We extracted a spectrum from the inner 3 arcmin (or 79 kpc) of the cluster (but excluding the point source) for comparison with the ASCA spectrum of Johnstone, Fabian & Taylor (1998). This region is expected to contain most of the mass deposition if a classical cooling flow is present (Johnstone, Fabian & Taylor 1998). We have fitted a range of models to this region; the results are presented in Table 2. Initially we fitted a single temperature `mekal` model affected only by (freely fitting) Galactic absorption (Model 1). This is our baseline model for the region.

Adding in a second `mekal` component (Model 2) in which the metallicity is linked to the first component reduces the chi-square value to 303.9 for 203 degrees of freedom and gives a significantly better fit (F-test significance=$1-1.9\times10^{-5}$).

Next we have substituted a cooling flow model for the second `mekal` component (Model 3) in which the upper temperature and metallicity of the cooling flow are tied to that of the `mekal` component, and the lowest temperature in the cooling flow model is below the *Chandra* band. Although this model is not a better fit than the two-temperature model in terms of the chi-square statistic, it only introduces one further fit parameter instead of two for Model 2 and an F-test shows the rediction in chi-square for this model to have a greater level of significance ($1-6.4\times10^{-6}$). The mass deposition rate fits to $8.1\pm1.3\,{\rm M}_\odot\,{\rm yr}^{-1}$. (Note that for comparison with previous values of mass deposition rate published by Johnstone, Fabian & Taylor (1998) this value should be doubled to account for the different assumed value of $H_0$.)

Finally, allowing the lower temperature of the cooling flow to be a free parameter allows chi-square to drop further to 302.8. There is an F-test probability of 0.15 of obtaining such a large drop in chi-square if the additional fit parameter were not required. The allowed mass deposition rate is now $12.7^{+3.9}_{-2.8}\,{\rm M}_\odot\,{\rm yr}^{-1}$. In Fig. 10 we show contours of constant C-statistic in the mass depostion rate / lower temperature plane. The three contours have Δ C-statistic = 2.3, 4.61 and 9.21 which correspond to 68, 90 and 99 per cent confidence regions for two interesting parameters.

Johnstone, Fabian & Taylor (1998) performed a surface brightness deprojection of the *ROSAT* HRI data. Within the central

3 arcmin (110 kpc in $H_0 = 50$, $q_0 = 0$ used in that paper), a mass deposition rate of $45-50\,M_\odot\,yr^{-1}$ was found. Scaling these values to our current cosmology would give a value of $22-25\,M_\odot\,yr^{-1}$, around a factor of three higher than fitted in this section when the gas is allowed to cool to very low temperatures. Similar results have been found for many other clusters by e.g. Peterson et al. (2001), Peterson et al. (2003), Kaastra et al. (2004). a lower cutoff temperature to the cooling gas proposed. At a cutoff temperature of around $\sim 0.8$ keV agreement with the deprojection mass deposition rates is achieved, albeit with a poor chi-square value. We note that 0.8 keV is the lowest temperature directly observed in the `projct` fits of section 4.2.

The problem remains as to why the gas appears to cool by about a factor of $\sim 2.5$ yet not any further and does not accumulate at the lower temperature.

## 5 DISCUSSION

So far we have considered heating in Abell 3581 only from the point of view of balancing the cooling from the ICM in the core of the cluster. However, there is a more global property of clusters that shows that heating has been important. The observed luminosity/temperature ($L_x/T_x$) relation for clusters, where $L_x \propto T_x^3$ (e.g. Arnaud & Evrard 1999) rather than $T_x^2$ as expected if only gravitational heating is involved (Kaiser 1986), indicates that some form of extra heating has taken place. The level corresponds to about 2-3 keV per particle (e.g. Wu et al. 2000). Low temperature clusters and groups show a large dispersion in the $L_x/T_x$ relation (Helsdon & Ponman 2000), which may mean that although heating is widespread, it is not the same in all objects. One possible origin for the heating, which has been suggested by many authors, is the radio source which is often associated with the central galaxy.

We have measured the unabsorbed X-ray luminosity in the central 60 kpc of both the Perseus cluster and Abell 3581 (excluding the point sources) and find values of $1.5\times10^{44}\,erg\,s^{-1}$ and $1.4\times10^{43}\,erg\,s^{-1}$ respectively in the 0.3-10 keV band, so the Perseus cluster is factor of ten brighter than PKS 1404-267 in this region. By comparison, the 1.4 GHz radio luminosity of the inner two radio lobes in the Perseus cluster is $2.0\times10^{24}\,W\,Hz^{-1}$ while the 1.4 GHz radio luminosity of the lobes in PKS 1404-267 is $2.5\times10^{23}\,W\,Hz^{-1}$, showing that the distributed radio power in the Perseus cluster is also a factor of ten brighter than in PKS 1404-267.

Abell 3581 is therefore particularly interesting as it is a low temperature cluster with a strong radio source where heating seems not to have been effective, even close to the active nucleus. Roychowdhury et al. (2004) have suggested that heating by the AGN should also affect the entropy profile of a cluster beyond the coolest parts. Even if the radio source has offset radiative cooling in the very innermost regions, it is clear that it has not had a strong influence on the gas entropy at $0.1R_{200}$, compared with similar low temperature clusters.

Various explanations for this are possible. a) The radio source may be very young compared with the radiative cooling time of hundreds of Myrs, in which case radiative cooling would have dominated in the past. However, no rapidly cooling cluster has yet been found elsewhere. b) The major heating phase in clusters may have occurred 5 or more billion years ago, beyond $z \sim 1$, when the central active galaxy or galaxies were much more important. This may have been a variable process which has left some clusters without significant heating. c) Perhaps Abell 3581 is particularly old and thus dense, and has had few recent mergers. Cooling in its high density core may absorb all the kinetic energy produced by the present active nucleus so that little is available for the rest of the gas. d) The dense core may have been introduced into the cluster as a result of a merger, or e) The dense cool core may have caused the moderately powerful radio source by more effectively fuelling the central black hole. Radio source heating as inferred for the Perseus cluster (by the dissipation of sound waves; Fabian et al. 2003) may also apply, and scale, to Abell 3581.

The core of Abell 3581 appears to be similar to that of the Perseus cluster, except that it is about an order of magnitude less luminous and has a temperature that is about one third of that in the Perseus cluster. Somehow the core has avoided the heating, or at least the effects of heating, common to most other low temperature clusters and groups.

## ACKNOWLEDGMENTS

ACF acknowledges support by the Royal Society. We thank J. Sanders for the use of his accumulative smoothing / contour binning software and many helpful discussions. We also thank an anonymous referee for helpful comments.

## REFERENCES

Allen S.W., Schmidt, R.W., Fabian A.C., 2001, MNRAS, 328, L37
Anders E., Grevesse N., 1989, Geochimica et Cosmochimica Acta, 53, 197
Arnaud K.A., 1996, in Jacoby G., Barnes J., eds, ASP Conf. Series volume 101, Astronomical Data Analysis Software and Systems V, Astron. Soc. Pac., San Francisco, p.17
Arnaud M., & Evrard A.E., 1999, MNRAS, 305, 631
Barnes D.G., Nulsen P.E.J., 2003, MNRAS 343, 315
Bettoni D., Falomo R., Fasano G., Govoni F., 2003, A&A 399, 869
Binney J., Tabor G., 1995, MNRAS, 276, 663
Bondi H., 1952, MNRAS 112, 195
Buote D.A., Fabian A.C., 1999, MNRAS, 310, 483
Burns J.O., Loken C., Gomez P., Rizza E., Bliton M., Ledlow M., 1997, in Soker N., ed, ASP Conf. Series volume 115, Galactic Cluster Cooling Flows, Astron. Soc. Pac., San Francisco, p.21
Cash W., 1979, ApJ, 228, 939
Churazov E., Brüggen M., Kaiser C.R., Böhringer H., Forman W., 2001, ApJ, 554, 261
Cole S., Lacey C., 1996, MNRAS, 281, 716
Conselice C.J., Gallagher J.S. III, Wyse R.F.G., 2001, AJ 122, 2281
Danziger I.J., Focardi P., 1988, in Fabian A.C., ed, NATO ASI Series, Cooling Flows in Clusters and Galaxies. Kluwer Academic Publishers, Dordrecht, p.133.
Davis J.E., 2001, ApJ, 562, 575.
Di Matteo T., Johnstone R., Allen S., Fabian A., 2001, ApJ, 550, 19
Di Matteo T., Allen S.W., Fabian A.C, Wilson A.S., Young A.J., 2003, ApJ, 582, 133
Fabian A.C., Mushotzky R.F., Nulsen P.E.J., Peterson J.R., 2001, MNRAS, 321, L20
Fabian A.C., Sanders J.S., Allen S.W., Crawford C.S., Iwasawa

K., Johnstone R.M., Schmidt R.W., Taylor G.B., 2003, MNRAS, 344, L43
Hartmann D, Burton W.B., 1997, Atlas of Galactic Neutral Hydrogen, Cambridge University press, Cambridge, UK
Helsdon S.F., Ponman T.J., 2000, MNRAS, 319, 933
Johnstone R.M., Fabian A.C., Nulsen P.E.J., 1987, MNRAS, 224, 75
Johnstone R.M., Fabian A.C., Taylor G.B., 1998, MNRAS, 298, 854
Johnstone R.M., Allen S.W., Fabian A.C., Sanders J.S., 2002, MNRAS, 336, 299
Kaastra J.S., Tamura T., Peterson J.R., Bleeker J.A.M., Ferrigno C., Kahn S.M., Paerels F.B.S., Piffaretti R., Branduardi-Raymont G., Böhringer H., 2004, A&A, 413, 415
Kaiser N., 1986, MNRAS, 222, 323
Liedahl D.A., Osterheld A.L., Goldstein W.H., 1995, ApJ, 438, L115
Lloyd-Davies E.J., Ponman T.J., Cannon D.B., 2000, MNRAS, 315, 689
Pellegrini S., Baldi A., Fabbiano G., Kim D.-W., 2003, ApJ, 597, 175
Peterson J.R., Paerels F.B.S., Kaastra J.S., Arnaud M., Reiprich T.H., Fabian A.C., Mushotzky R.F., Jernigan J.G., Sakelliou I., 2001, A&A, 365, 104
Peterson J.R., Kahn S.M., Paerels F.B.S., Kaastra J.S., Tamura T., Bleeker J.A.M., Ferrigno, C., Jernigan J.G., 2003, ApJ, 590, 207
Ponman T.J., Sanderson A.J.R., Finoguenov A., 2003, MNRAS, 343, 331.
Pratt G.W., Arnaud M., 2003, A&A, 408, 1
Roychowdhury S., Ruszkowski M., Nath B.B., Begelman M.C., 2004, astro-ph/0401161
Sanders J.S., Fabian A.C., Allen S.W., Schmidt R.W., 2004, MNRAS, 349, 952
Sanderson A.J.R., Ponman T.J., Finoguenov A., Lloyd-Davies E.J., Markevitch M, 2003, MNRAS, 340, 989
Stark A.A., Gammie C.F., Wilson, R.W., Bally J., Linke R.A., Heiles C., Hurwitz M., 1992, ApJS, 79, 77
Tozzi P., Norman C., 2001, ApJ, 546, 63.
Wu K.K.S., Fabian A.C., Nulsen P.E.J., 2000, MNRAS, 318, 889

This paper has been typeset from a TEX/ LATEX file prepared by the author.